A new approach to follow the formation of iron oxide nanoparticles synthesized by thermal decomposition

A new approach to follow the formation of iron oxide nanoparticles synthesized by thermal decomposition

Sarah Belaïd[1]**, Sophie Laurent**[1]**, Marjorie Vermeech**[2,3]**,
Luce Vander Elst**[1]**, David Perez-Morga**[2,3] **and Robert N Muller**[1,3]

[1] Department of General, Organic and Biomedical Chemistry, NMR and Molecular Imaging Laboratory,
University of Mons, B-7000 Mons, Belgium
[2] Laboratory of Molecular Parasitology, Institute of Molecular Biology and Medicine (IBMM),
Université Libre de Bruxelles, B-6041 Gosselies, Belgium
[3] Center for Microscopy and Molecular Imaging (CMMI), B-6041 Gosselies, Belgium

E-mail: sarah.belaid@umons.ac.be and robert.muller@umons.ac.be

Abstract
A novel way has been proposed to follow the formation of nanocrystalline magnetite. Iron oxide nanoparticles were synthesized by the thermal decomposition of $Fe(acac)_3$ in the presence of oleic acid and oleylamine surfactants at high temperature. The species produced during the synthetic process are characterized through their effects on the proton nuclear magnetic relaxation of the reaction medium and their sizes. As shown by transmission electron microscopy, photon correlation spectroscopy and x-ray diffraction, the diameter of nano-objects increases when the time synthesis is longer. Magnetic properties evaluated by nuclear magnetic resonance (NMRD profiles, T_1 and T_2 measurements) were correlated with the size parameters.

[S] Online supplementary data available from stacks.iop.org/Nano/24/055705/mmedia

(Some figures may appear in colour only in the online journal)

1. Introduction

Magnetic nanoparticles are attractive as medical and therapeutic probes in biomedical applications. In particular, iron oxide nanoparticles (NPs) are promising candidates for biomolecular tagging, imaging, sensing and separation [1–3]. These materials have interesting magnetic properties, closely related to their chemical and physical characteristics, which depend on the synthetic method [4]. Iron oxide nanoparticles with a core size inferior to magnetic domains of the bulk magnetite [5, 6] and made of a single crystal possess a superparamagnetic behavior [7, 8] and are called superparamagnetic iron oxide nanoparticles (SPION) [9, 10]. SPION suspensions are characterized by an absence of permanent magnetization (remanence) and hysteresis [11]. SPION can be produced by two main synthetic procedures carried out in aqueous or organic media. A commonly used

method is the Massart synthesis [12, 13], an aqueous phase procedure. The process consists of the coprecipitation of iron precursors, Fe^{2+} and Fe^{3+} ions (from $FeCl_2$ and $FeCl_3$), in a basic medium. Although this precipitation method is suitable for large-scale production of magnetic NPs, it requires the careful adjustment of the reaction parameters [14] and often results in a rather broad size distribution [15] of the NPs. SPION can be easily further dispersed in an aqueous medium by acidic treatment [16]. For future medical applications, the biodistribution of the materials will be crucial; it depends on the chemical and physical characteristics of the NPs, mainly on their size and their size distribution [17, 18]. For a few years, thermal decomposition has been more widely used [19]. It involves the decomposition of inorganic iron precursors (iron(III) acetylacetonate, iron(0) pentacarbonyl, . . .) in the presence of the surfactants (oleic acid, oleylamine, . . .) in an organic medium at high temperature ($\geq 200\,^\circ$C) [20, 21].

NPs obtained in this way have a high magnetization, a high crystallinity and a narrow size distribution. However, for biomedical applications, it is necessary to transfer the iron oxide nanoparticle suspensions to an aqueous medium and to cover them with an appropriate coating. Over the past few years, many strategies have been developed to modify the nanoparticle surface [22–24]. The choice of the coating procedure is important to prevent the agglomeration of nanoparticles and to allow their vectorization. According to Lamer theory [6, 25, 26], the nucleation and growth steps must be separated to produce monodisperse nanoparticle suspensions, but actually, little information is reported in the literature on the thermal decomposition. In the current investigation, we study the kinetics of the production of iron oxide nanoparticles by thermal decomposition of $Fe(acac)_3$ in the presence of the surfactants at high temperature. The formation of the nanoparticles was followed by NMR and size measurements throughout the synthesis. To our knowledge, this is the first study which discusses the relaxometric and size behaviors during the formation of NPs synthesized by thermal decomposition in an organic medium.

2. Experimental details

2.1. Materials

Iron(III) acetylacetonate (97%), 1,2-hexadecanediol (90%), oleic acid (90%), oleylamine (70%), benzylether (99%) and iron standard for ICP (TraceCerd©) were purchased from Sigma-Aldrich (Bornem, Belgium) and used as received. Heptane (99%) and ethanol (96%) were purchased from Acros Organic (Geel, Belgium) and used without purification.

2.2. Syntheses

The synthesis of iron oxide nanoparticles was based on the procedure published by Sun *et al* [27]. In a typical experiment, 2 mmol of iron(III) acetylacetonate was dissolved in 10 ml of benzylether and heated to 80 °C for 30 min under stirring. Alternatively, 10 mmol of 1,2-hexadecanediol, 6 mmol of oleic acid, and 6 mmol of oleylamine were added to 10 ml of benzylether in a three-neck round-bottom flask under magnetic stirring and a nitrogen atmosphere. This mixture was heated to 200 °C for 60 min in order to stabilize the temperature and to melt the reactants. The diluted solution of iron precursor was then added by rapid injection in the three-neck round-bottom flask. The reaction mixture was then heated to 200 °C under magnetic stirring and a nitrogen atmosphere for 30 min. The mixture was then gradually heated to reflux with a heating rate of 2.5 °C min^{-1} and was kept under reflux for 30 min. During this sequence, six aliquots of around 1 ml were taken, as shown in figure 1; three of them (A, B and C) correspond to the samples taken after the injection of iron precursors solution while the reaction was kept at 200 °C; while the other three (D, E and F) correspond to the samples taken when the temperature was equal to 300 °C. These samples were washed as described in the following paragraph. During the synthesis, the initial
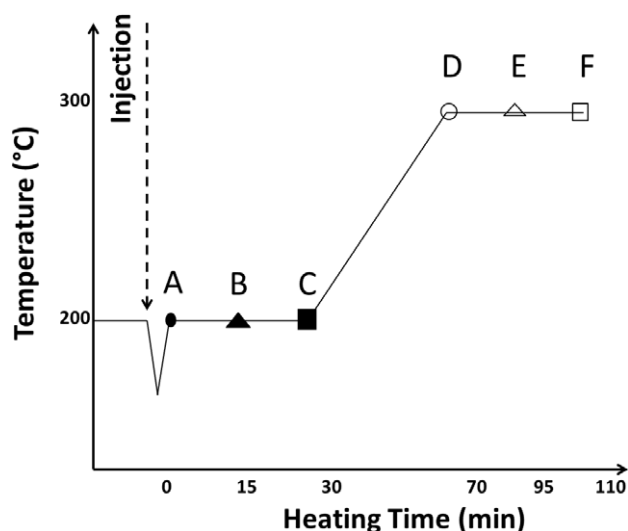
Figure 1. Heating sequence of the synthesis of iron oxide nanoparticles produced by thermal decomposition. After the injection of iron precursor, six aliquots were taken at various delays during the process: three at 200 °C (●, ▲ and ■) and three at 300 °C (○, △ and □).

reddish-brown solution became a brownish-black suspension. At the end of the reaction period, this dark mixture was cooled down to room temperature by replacing the heating source by a cool water bath.

2.3. Purification

40 ml of ethanol was added to the mixture solution at room temperature. The black materials precipitated because the products were coated with hydrophobic surfactants (oleic acid). The solid was isolated by centrifugation (8000 rpm, 8 min) and the supernatant was discarded. The precipitate was dissolved in 20 ml of *n*-heptane and the mixture was centrifuged (8000 rpm, 8 min) again to remove any undispersed residue. This washing step was repeated three times. Finally, the nanoparticles were dispersed in 20 ml of *n*-heptane for long-term storage.

2.4. Characterization

2.4.1. Inductively Coupled Plasma-Atomic Emission Spectroscopy (ICP-AES). Dosage of iron was performed by ICP-AES on a Jobin Yvon JY70$^+$ instrument (Longjumeau, France). The total amount of iron in the NPs suspensions determined by these ICP measurements was used in the calculations of the relaxometric properties of the NPs. All samples were prepared for analysis as follows. Suspensions of iron oxide nanoparticles (typically 0.2 ml) were added in concentrated HNO_3 (0.5 ml). The mixture was heated to 80 °C for 30 min in a water bath. The solution was immediately removed from the heat and allowed to cool at room temperature. Samples were supplemented with distilled water up to a volume of 5 ml. This procedure transforms iron(II) to iron(III) by acidic oxidation and allows the

determination of the total amount of iron. An iron standard solution for ICP (1000 mg ml^{-1} of iron in nitric acid) was used to obtain a calibration curve. The same procedure was used for the determination of the residual iron concentration of the supernatant solution during the washing step.

2.4.2. Nuclear magnetic resonance. ^{1}H NMRD profiles (nuclear magnetic resonance dispersion) were obtained at 37 °C using a Stelar fast field cycling relaxometer (Mede, Italy) over a range of magnetic fields extending from 0.25 mT to 0.94 T (0.01–40 MHz). The theoretical adjustment of the NMRD profiles was performed with classical relaxation models [28–30] assuming a diffusion coefficient of *n*-heptane of 3.53 10^{-5} cm^2 s^{-1} [31, 32]. Measurements of T_1 and T_2 relaxation times were performed at 37 °C on a Bruker Minispec systems mq60 (Karlsruhe, Germany) working at 60 MHz (1.41 T). All samples were dispersed in an organic medium (*n*-heptane).

2.4.3. Transmission electron microscopy. TEM was used to obtain detailed morphological information on the samples and was carried out on a Microscope Fei Tecnai 10 operating at an accelerating voltage of 80 kV (Oregon, USA). The samples were prepared by placing a drop of diluted solution of iron oxide nanoparticle suspension in heptane on a carbon-coated copper grid (300 mesh) allowing the liquid to dry in air at room temperature. The statistical treatment of the TEM images was performed by iTEM analysis (Münster, Germany) on multiple images for each sample. The mean diameter, the standard deviation and the polydispersity index (PDI) were calculated by measuring the diameter of particles. The number of nanoparticles counted ranges from 250 to 1000.

2.4.4. Photon Correlation Spectroscopy (PCS). Measurements of the size distribution of the nanoparticle suspensions dispersed in *n*-heptane were performed on a Zetasizer NanoS PCS from Malvern instrument (Worcestershire, UK). Hydrodynamic diameters were measured on the suspension after the purification steps. The parameters used were 0.39 mPa s at 25 °C for the viscosity of the *n*-heptane and the refractive index of iron oxide nanoparticles is about 2.42.

2.4.5. X-ray diffraction (XRD). The x-ray diffraction experiments were performed on a D5000 Siemens diffractometer (Karlsruhe, Germany) using Cu Kα radiation (λ = 0.154 056 nm). The scattering intensities were measured over an angular range of 20° < 2Θ < 120° for all aliquots. One measurement was recorded every 0.05° and the duration of the recording is about 25 s for each point of the XRD patterns. The analysis was recorded at room temperature. By adding ethanol in magnetic suspensions, the nanoparticles precipitate. The supernatant was discarded by magnetic separation and the precipitate was dried under vacuum for three days. The nanoparticle powders were obtained by this procedure.

3. Results and discussion

The nanoparticles of iron oxide were produced by thermal decomposition at high temperature. In the present investigation, the thermal decomposition of iron(III) acetylacetonate in the presence of oleic acid, oleylamine and 1,2-hexadecanediol in benzylether was chosen. During the synthesis, two different heating plateaus were used for the NPs formation steps: at 200 °C and at 300 °C. It is usually assumed that the decomposition of iron(III) acetylacetonate in iron precursors is promoted by the presence of 1,2-hexadecanediol and by high temperature. The diol derivative, known for its reducing properties, turns the trivalent iron into divalent iron [33, 34]. These two oxidation states are required to produce iron oxide nanoparticles. The temperature destabilizes the iron(III) acetylacetonate and the diol replaces the acetylacetonate group to form a primary species. During the synthesis, oleic acid is used to prevent the agglomeration between the nanoparticles and to control the growth of the nano-objects. At the same time, oleylamine is used to form deprotonated oleic acid since it has been shown that the carboxylate group is more reactive than the carboxylic acid group for the surface of iron oxide NPs [26]. Oleate molecules can slow down the kinetics of nanoparticle formation at the beginning of the synthesis. Samia *et al* reported the existence of complexes between ligand and metal. In particular, metal–oleate complexes were isolated and indicated by mass spectrometry [35]. In the case of an iron precursor in the presence of hexadecanediol and oleic acid, we assumed that iron bound to diol or oleate molecules can exist at the same time and both species can control the nanoparticle formation. Rocchioccioli-Deltcheff *et al* have proved by infrared spectroscopy that the carboxylate group of oleate molecules is chelated to iron according to a bidentate configuration [36]. Two phenomena of ripening are reported: Ostwald and digestive ripening [37–39]. Both models have dramatically opposite impacts on nanocrystal polydispersity. Ostwald ripening allows for large nanocrystals to grow at the expense of small ones, while digestive ripening involves the propagation of small nanocrystals at the cost of the larger. It is difficult to determine the ripening process; therefore, in this work, we try to better understand the ripening process thanks to the use of a large variety of characterizations.

### 3.1. Determination of residual iron concentrations

For each batch, the initial concentration of iron precursors used is equal to 0.1 M. After the purification procedures, supernatant solutions obtained were kept and the iron content of these solutions was analyzed by inductively coupled plasma (ICP). The residual iron ion concentrations decrease from 4.8 to 0.05 mM for the aliquot A–F (figure 2). These values are low compared to the initial concentration of iron(III) precursors. It can therefore be estimated that over 90% of the initial iron(III) ions react during the first moments of the synthesis. Most iron precursors were consequently transformed into nanoparticles or nuclei. It can thus be assumed that the nucleation proceeds very rapidly, maybe

Table 1. Saturation magnetization M_s, particles diameter measured by NMRD, TEM, PCS and XRD and polydispersity index (PDI). (Note: M_s were extracted from NMRD profiles, D^{NMRD} of A, B and C samples have to be considered as a rough estimation and PDI were calculated by statistical treatment with TEM images.)

| Sample | Saturation magnetization M_s (A m^2/kg iron) | Diameter | | | | Polydispersity index |
		D^{NMRD} (nm)	D^{TEM} (nm)	D^{PCS} (nm)	D^{XRD} (nm)	
A	8.5	(7.9 ± 0.1)	1.7 ± 0.8	5.4 ± 0.3	/	1.5
B	7.3	(8.7 ± 0.1)	4.8 ± 2.4	6.2 ± 0.3	3.7	1.5
C	9.2	(9.3 ± 0.1)	5.2 ± 1.9	7.5 ± 0.3	2.9	1.3
D	43.5	9.9 ± 0.1	5.5 ± 2.4	14.2 ± 0.3	5.5	1.4
E	45.3	9.9 ± 0.1	7.0 ± 1.6	12.4 ± 0.3	5.4	1.2
F	43.7	10.2 ± 0.1	6.8 ± 1.9	14.2 ± 0.3	5.5	1.2
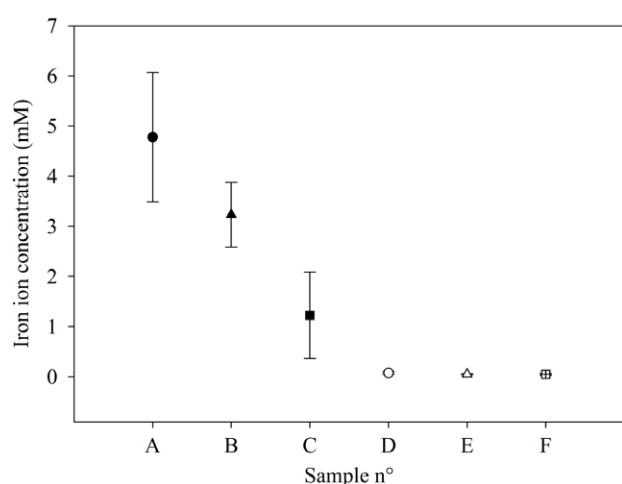
Figure 2. Residual iron concentration of the supernatant solution measured for each aliquot: A (●), B (▲), C (■), D (○), E (△) and F (□).
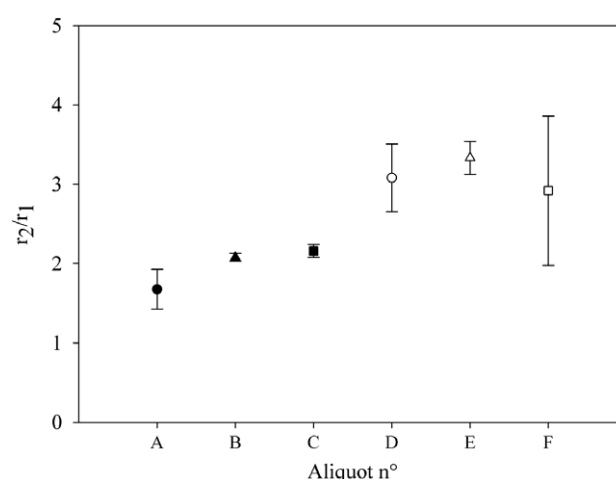
Figure 3. At 37 °C, the ratio between the transversal and the longitudinal relaxivities r_2/r_1 recorded at 60 MHz in *n*-heptane medium for samples A (●), B (▲) and C (■) (synthesized at 200 °C) and for samples D (○), E (△) and F (□) (synthesized at 300 °C).

during the first few seconds or minutes of the synthesis. A high number of nuclei are formed in the first instant of the synthesis and this step is generally called 'burst nucleation'. The growth of the size of the nano-objects is then observed, as shown by the results obtained by TEM, PCS and XRD measurements (table 1). One hypothesis is that a partial dissolution phenomenon of primary species or nuclei exists. As a result, iron is available to react with the surface of non-dissolved primary species. Another hypothesis is that the primary species associate together to form nanoparticles with larger size [6, 25, 40].

3.2. Nuclear magnetic resonance properties

To obtain more detailed information on the thermal decomposition process and on the formation of iron oxide nanoparticles, nuclear magnetic resonance measurements were performed on the samples obtained during the heating process. Samples were taken during the synthesis as described above (see figure 1). After the washing steps (as previously described in section 2), each aliquot was dispersed in *n*-heptane and was analyzed by relaxometry. The measurements were performed at 37 °C and at 1.41 T (60 MHz). Longitudinal and transversal relaxivities (r_1 and

r_2) measured in *n*-heptane are defined as the increase of the relaxation rate of *n*-heptane induced by one millimole per liter of iron. The diamagnetic contribution (R_1 and R_2) of *n*-heptane at 37 °C and at 60 MHz are 0.39 s^{-1} and 0.46 s^{-1} respectively. Figure 3 shows that the ratio r_2/r_1 at 60 MHz increases gradually with the heating time. At the beginning of the heating program corresponding to the temperature of 200 °C, r_2/r_1 is equal to 1.6. This ratio increases to 2.1 due to formation of nuclei or nanoparticles in the mixture (sample B and C). For sample D, corresponding to the earlier time of the 300 °C, r_2/r_1 increases to 3. This ratio remains almost constant for samples E and F.

These results were confirmed by the NMRD profiles (figure 4) which display the evolution of proton longitudinal relaxivity as a function of the applied field. It is known that the shape of the NMRD profile of magnetic nanoparticle suspensions is governed (1) by the size, the crystallinity and the magnetization of the magnetic cores, (2) by the diffusion of solvent near the iron oxide cores of the particles, and (3) by the interaction between superparamagnetic cores, as they affect the anisotropy energy [41, 42].

NMRD profiles were recorded for all samples. The results show that samples A, B and C have very low longitudinal relaxivities compared to samples D, E and F. All profiles are
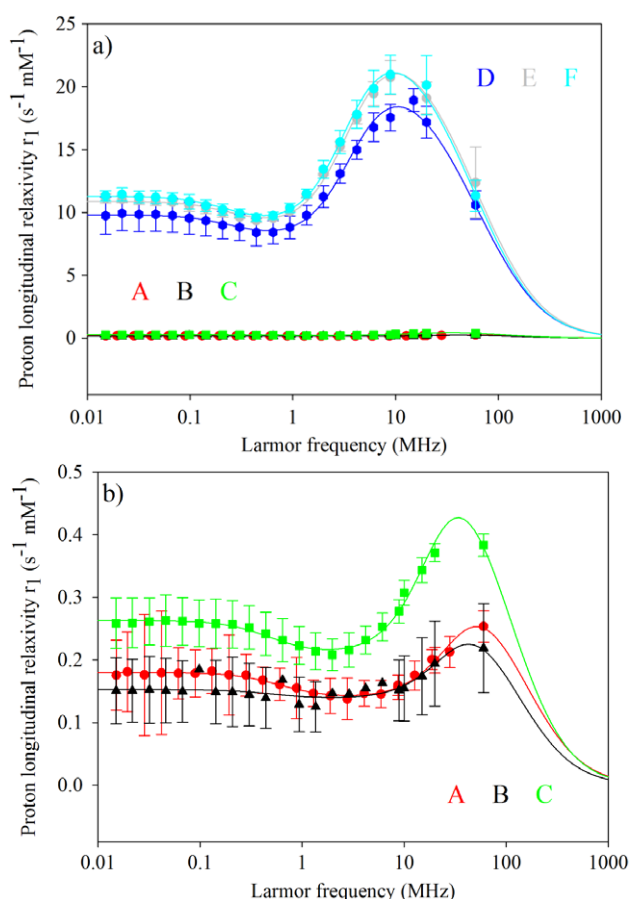
Figure 4. (a) ^{1}H relaxation profiles, recorded at 37 °C in *n*-heptane, for samples A to F (samples taken during the synthetic process). The solid lines correspond to the simulation according SPM theory and (b) Blow up of the NMRD profiles of A–C.

however typical of paramagnetic and/or superparamagnetic iron oxide nanoparticles. At high field, the maximum proton longitudinal relaxivity r_1^{max} is observed around 10 MHz for the samples D–F. This longitudinal relaxivity maximum increases with the heating time at 200 °C and its position moves towards lower proton Larmor frequencies (samples A, B and C). The relative differences between samples D, E and F (at reflux) are lower than between samples A, B and C. At low field, a small dispersion is observed for samples D, E and F (figure 4(a)). This is typical of iron oxide nanoparticles with a size smaller than magnetic domains of bulk magnetite [5, 6, 43, 44]. In figure 4(b), it can be seen that samples A, B and C also present dispersion at low field, corresponding to superparamagnetic iron oxide nanoparticles with a small magnetic core. The experimental relaxivity profiles of samples A to F were fitted using the usual superparamagnetic models theory [28–30] (SPM) (figure 4) adapted to be applied to suspensions in *n*-heptane of which the diffusion coefficient is 3.53 10^{-5} cm^2 s^{-1} [32, 45]^4 at 37 °C. These results allow the following conclusions: firstly, the increase of r_2/r_1 indicates that the structure of the compound changes with

---

^{4} The diffusion coefficient of *n*-heptane was measured by NMR techniques and was compared with the literature measurement.

the heating time and that the nanoparticle size becomes larger, as shown by the high values of r_2 measured. This conclusion is confirmed by the appearance of the hump at lower frequency (around 10 MHz) for samples D, E and F as compared to samples A, B and C (around 70 MHz). Secondly, two behaviors were observed during the synthetic process. Depending on the temperature of the solution, the NMRD profiles show very low relaxivity when the temperature of the reaction mixture is 200 °C, whereas at 300 °C the NMRD profiles are typical of high relaxivity superparamagnetic iron oxide nanoparticles. Hence, the lower temperature step is thought to correspond to the nucleation phase since the proton longitudinal relaxivity remains low. During the second step, the size of the initially small nuclei increases to form larger nanoparticles and corresponds to the growth step. Table 1 shows the values of the relaxometric diameter D^{NMRD} (which represents the shorter distance between the magnetic core and the *n*-heptane molecule) and the saturation magnetization M_s extracted by the theoretical fitting of the NMRD profiles. The NMR diameter of the magnetic core obtained is close to 10 nm for the samples heated at 300 °C (between 9.9 and 10.2 nm). The first three values of NMRD diameters (A, B and C aliquots) are much higher than the sizes obtained by TEM and PCS. These NMRD data must be considered as rough values since the outer sphere relaxation theory was developed for crystalline magnetic nanomaterials. X-ray diffraction measurements show that the crystalline phase of these three samples is quite low (see below). The saturation magnetization obtained from the fitting of NMRD profiles increases as a function of the heating time; this parameter depends mainly on the size and the crystallinity of the nanomaterials. The theoretical M_s of the samples of the first plateau (aliquots A, B and C) are less than 10 A m^2 kg^{-1} of iron(III), whereas the samples taken at 300 °C (samples D, E and F) possess a high saturation magnetization (around 45 A m^2 kg^{-1} of iron). M_s of C and D samples are markedly different; the hypothesis explaining this observation is that the crystallinity grows when the synthetic temperature is at 300 °C without an increase in size of the nanoparticle. As compared with XRD measurements, well defined peaks were observed when the heating time was longer. In addition, the size characterization by TEM, PCS and XRD shows the same observations.

3.3. Size measurements by PCS, TEM and XRD

All aliquots were analyzed by size measurements with photon correlation spectroscopy (PCS), transmission electron microscopy (TEM) and x-ray diffraction (XRD). Table 1 compares the size results obtained by different characterizations.

3.3.1. Transmission electron microscopy.
Figure 5 shows the TEM images for each aliquot. The average diameter, the standard deviation and the polydispersity index (PDI) were extracted by a size statistical treatment of TEM images (table 1). The average diameter of the particle core increases from 1.7 to 6.8 nm during the heating process (the size
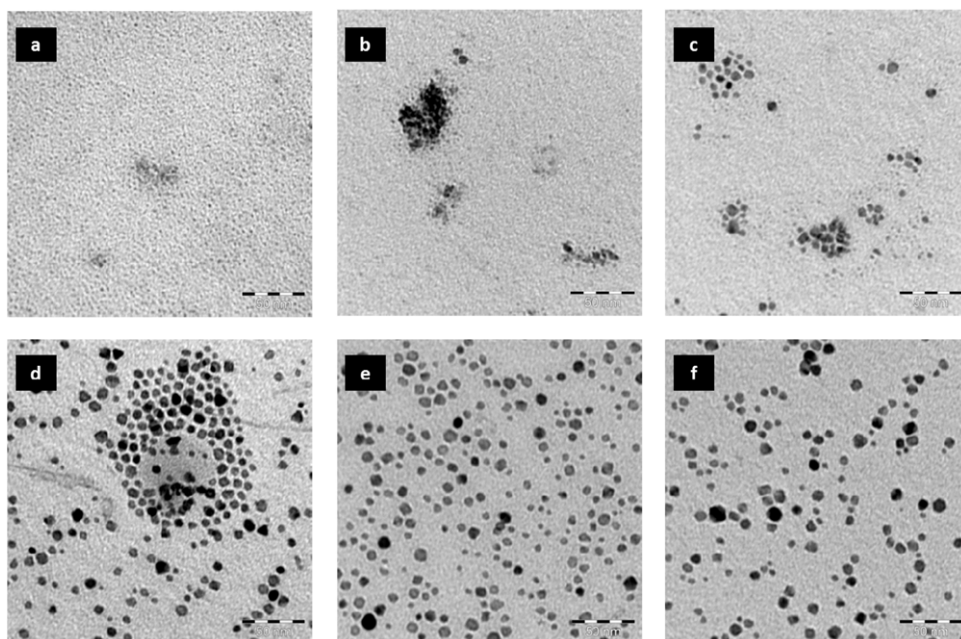
Figure 5. (a)–(c) TEM images of A, B and C: samples heated to 200 °C. (d)–(f) TEM images of D, E and F: samples heated to 300 °C.

histogram of each sample is described in supplementary data files available at stacks.iop.org/Nano/24/055705/mmedia). The mean size is smaller than 5 nm for samples A and B. From sample C, an increase of the nanoparticle size is observed and a value close to 7 nm is obtained for samples E and F.

TEM and relaxometry results therefore lead to the same conclusions: when the temperature and the heating time increase, the mean diameter also increases in the same way. In addition, the PDI decreases from 1.5 to 1.2 with time. At the end of the synthesis, the PDI results show that the dispersion index of the nanoparticles is low and the size distribution is narrow. The nanoparticle growth seems thus to be governed by digestive ripening, since this model has been established as a very convenient route to obtain monodisperse nanoparticles from polydisperse materials when the system is heated at reflux with an excess of ligand [37, 38]. The decrease of PDI shows that the small nanoparticles grow preferentially as compared to the large size ones to obtain a final uniform size.

3.3.2. Photon correlation spectroscopy. PCS was used to measure the hydrodynamic diameter of the nanoparticles. The PCS diameter is generally higher than the TEM size because TEM measures the magnetic core size (D^{TEM}) whereas the PCS measures the nanoparticle size with their coating and their solvation layer (D^{PCS}), as illustrated in figure 6. The PCS diameter increases from 5.4 to 14.2 nm during the synthesis process whereas the TEM diameter goes from 1.7 to 6.8 nm (table 1). The difference between these two techniques can be assumed to correspond to the thickness of the oleic acid coating (C18 carbon chains) of the nanoparticles and the heptane solvation layer. The oleic acid likes hydrophobic solvents such as *n*-heptane, therefore the carboxylic function of oleic acid interacts on the surface of the nanoparticles and the long carbons chains of this surfactant are extended
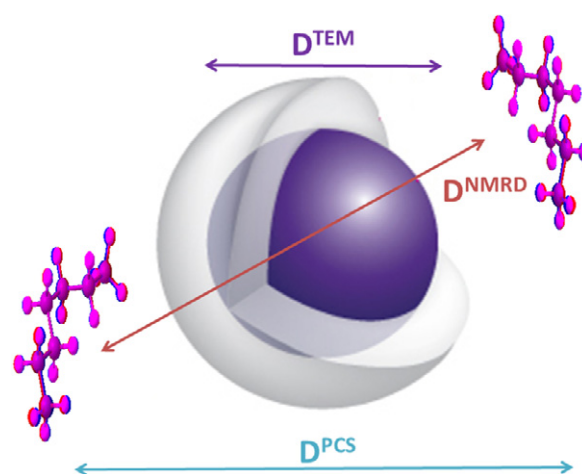
Figure 6. Schematic representation of iron oxide nanoparticles coated with oleic acid; difference between D^{PCS}, D^{TEM} and D^{NMRD}.

within the solvent. In this case, the theoretical length of the hydrophobic coating is estimated as around 2.8 nm. The difference between TEM and PCS increases when the solution is heated at reflux. This can be explained by the excess of oleic acid used during the synthetic process. At high temperature, it is hypothesized that the diffusion of oleate complexes increases and that a large quantity of complexes deposit on the surface of the small nanoparticles with a subsequent formation of an oleate bilayer [45]. Gong *et al* have indeed confirmed the presence of two oleate layers on the nanoparticle surface by thermogravimetric analysis [46].

3.3.3. XRD measurements. X-ray diffraction was used to determine the crystal structure and the size of crystalline nanoparticles. Figure 7 shows those XRD results for
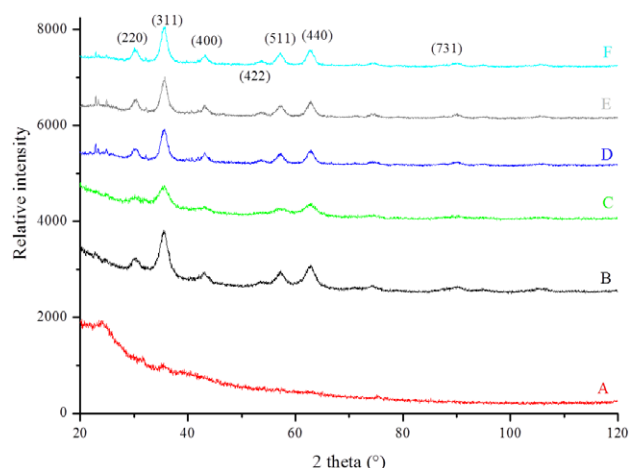
Figure 7. X-ray diffraction patterns of samples A to F with the theoretical positions of the characteristic XRD peak of magnetite.

all samples. The position and relative intensity of all diffraction peaks match well with both standard magnetite and maghemite powder diffraction data [47].

For sample A, no peak was observed in the analysis range ($2\theta = 15°–120°$), indicating that the nanoparticles or nuclei were not yet in a crystalline phase. In addition, between 15°and 40°, a large peak that corresponds to the amorphous phase of the nanomaterials was observed. The results show that this amorphous zone disappears with the heating time. From sample B, the characteristic peaks were observed and confirmed that the nano-objects begin to become crystalline. Moreover, the peak positions correspond well with the face-centered cubic structure, which is characteristic for both magnetite and maghemite, but the choice of the type of the material is difficult from the XRD data. The intensity of the 3 characteristic peaks increases when going from B to F, as shown in figure 7: values of 2θ at around 35°, 57°and 63°correspond to lattice faces of (311), (511) and (440) respectively. On the other hand, the size of crystal domains can be determined by the Sherrer formula [48]:

$$D \approx \frac{0.89\lambda}{\beta \cos\theta}$$

where λ is the wavelength of the XRD source (0.154 056 nm), θ is the diffraction angle, β is the full width at half maximum intensity of the peak, and D is the particle size. The diameter of the crystal was calculated from the peak of a lattice face of (311). The results are shown in table 1. The XRD diameter grows from 3.7 to 5.5 nm. The size of the crystal domains varies for samples taken at 200 °C (samples B and C), whereas it remains at the same higher value for samples D, E and F (around 5.5 nm). As explained above, samples C and D have very different values of saturation magnetization, but they have the same TEM diameters. The XRD results show that the crystalline size of sample C (2.9 nm) is smaller than for sample D (5.5 nm), therefore these observations explain the lower value of the saturation magnetization of sample C as compared to sample D (see nuclear magnetic resonance properties). The average particle diameter estimated from

Sherrer's formula is similar to the size obtained from TEM images, indicating that each individual particle is a single crystal.

4. Conclusions

To summarize, we have introduced a novel approach to follow the formation of iron oxide nanoparticles synthesized by the 'rapid injection' process at high temperature. The NMRD results afford new information on the nanoparticle formation. Analyses of aliquot solutions which are taken during the thermal decomposition process were characterized and verified by the NMR data (T_1 and T_2), NMRD profiles, TEM, PCS and XRD measurements. The first heating step (200 °C) gives low relaxivity, a small size and a low crystallinity of the nano-objects, whereas during the second heating step (300 °C) a high relaxivity, a high crystallinity and a larger size are obtained. The size of nanomaterials increases during the synthesis, whereas the polydispersity index decreases. The nanoparticle formation seems thus to agree with digestive ripening where the small nuclei increases to form final nanoparticles and the larger ones dissolve to favor the formation of smaller size nanoparticles. The data obtained by the different characterizations illustrated the modification of iron precursors to form the final iron oxide nanoparticles. This work demonstrated that it is necessary to heat the reaction mixture to 300 °C in order to obtain crystalline nanoparticles with high magnetic properties (relaxivity and saturation magnetization).

Acknowledgments

References

[1] Veiseh O, Gunn J W and Zhang M 2010 *Adv. Drug Deliv. Rev.* **62** 284–304
[2] Huang S H and Juang R S 2011 *J. Nanopart. Res.* **13** 4411–30
[3] Laurent S, Boutry S, Mahieu I, Vander Elst L and Muller N R 2009 *Curr. Med. Chem.* **16** 4712–27
[4] Roca A G, Morales M P, O'Grady K and Serna C J 2006 *Nanotechnology* **17** 2783–8
[5] Frenkel J and Doefman J 1930 *Nature* **126** 274–5
[6] Tartaj P, Morales M P, Veintemillas-Verdaguer S, González-Carreño T and Serna C J 2003 *J. Phys. D: Appl. Phys.* **36** R182
[7] Coey J M D 1971 *Phys. Rev. Lett.* **27** 1140–2

[8] Zysler R D, Romero H, Ramos C A, De Biasi E and Fiorani D 2003 *J. Magn. Magn. Mater.* **266** 233–42

[9] Dimitrov D A and Wysin G M 1994 *Phys.Rev.* B **50** 3077–84

[10] Can M M, Coşkun M and Fırat T 2011 *J. Nanopart. Res.* **13** 5497–505

[11] Chomoucka J, Drbohlavova J, Huska D, Adam V, Kizek R and Hubalek J 2010 *Pharmacol. Res.* **62** 144–9

[12] Lefebure S, Dubois E, Cabuil V, Neveu S and Massart R 1998 *J. Mater. Res.* **13** 2975–81

[13] Liu F, Laurent S, Fattahi H, Vander Elst L and Muller N R 2011 *Nanomedicine* **6** 519–28

[14] Forge D, Roch A, Laurent S, Tellez H, Gossuin Y, Renaux F, Vander Elst L and Muller N R 2008 *J. Phys. Chem.* C **112** 19178–85

[15] Behrens S 2011 *Nanoscale* **3** 877–92

[16] Sugimoto T and Matijević E 1980 *J. Colloid Interface Sci.* **74** 227–43

[17] Cho M, Cho W S, Choi M, Kim S J, Han B S, Kim S H, Kim H O, Sheen Y Y and Jeong J 2009 *Toxicol. Lett.* **189** 177–83

[18] Schlachter E K *et al* 2011 *Int. J. Nanomedicine* **6** 1793–800

[19] Frey N A, Peng S, Cheng K and Sun S 2009 *Chem. Soc. Rev.* **38** 2532–42

[20] Hyeon T, Lee S S, Park J, Chung Y and Na H B 2001 *J. Am. Chem. Soc.* **123** 12798–801

[21] Sun S and Zeng H 2002 *J. Am. Chem. Soc.* **124** 8204–5

[22] Jana N R, Earhart C and Ying J Y 2007 *Chem. Mater.* **19** 5074–82

[23] Herranz F, Morales M P, Roca A G, Vilar R and Ruiz-Cabello J 2008 *Contrast Media Mol. Imag.* **3** 215–22

[24] De Palma R, Peeters S, Van Bael M J, Van den Rul H, Bonroy K, Laureyn W, Mullens J, Borghs G and Maes G 2007 *Chem. Mater.* **19** 1821–31

[25] LaMer V K and Dinegar R H 1950 *J. Am. Chem. Soc.* **72** 4847–54

[26] Sugimoto T 1987 *Adv. Colloid Interface Sci.* **28** 65–108

[27] Sun S, Zeng H, Robinson D B, Raoux S, Rice P M, Wang S X and Li G 2003 *J. Am. Chem. Soc.* **126** 273–9

[28] Roch A, Gillis P, Ouakssim A and Muller N R 1999 *J. Magn. Magn. Mater.* **201** 77–9

[29] Roch A, Gossuin Y, Muller N R and Gillis P 2005 *J. Magn. Magn. Mater.* **293** 532–9

[30] Gillis P, Moiny F and Brooks R A 2002 *Magn. Reson. Med.* **47** 257–63

[31] Moore J W and Wellek R M 1974 *J. Chem. Eng. Data* **19** 136–40

[32] Fishman E 1955 *J. Phys. Chem.* **59** 469–72

[33] Shemer G, Tirosh E, Livneh T and Markovich G 2007 *J. Phys. Chem.* C **111** 14334–8

[34] Niederberger M and Garnweitner G 2006 *Chem. Eur. J.* **12** 7282–302

[35] Samia A C S, Schlueter J A, Jiang S J, Bader S D, Qin C-J and Lin X-M 2006 *Chem. Mater.* **18** 5203–12

[36] Rocchiccioli-Deltcheff C, Franck R, Cabuil V and Massart R 1987 *J. Chem. Res.* **5** 126–7

[37] Lee D-K, Park S, Lee J K and Hwang N-M 2007 *Acta Mater.* **55** 5281–8

[38] Zhang Q, Xie J, Yu Y and Lee J Y 2010 *Nanoscale* **2** 1962–75

[39] Dagtepe P and Chikan V 2012 *J. Phys. Chem.* C **114** 16263–9

[40] Den Ouden C J J and Thompson R W 1991 *J. Colloid Interface Sci.* **143** 77–84

[41] Meledandri C J, Stolarczyk J K, Ghosh S and Brougham D F 2008 *Langmuir* **24** 14159–65

[42] Roch A, Muller N R and Gillis P 1999 *J. Chem. Phys.* **110** 5403–11

[43] Koenig S H and Kellar K E 1995 *Magn. Reson. Med.* **34** 227–33

[44] Gossuin Y, Gillis P, Hocq A, Vuong Q L and Roch A 2009 *Wiley Interdisc. Rev. Nanomed. Nanobiotechnol.* **1** 299–310

[45] Yang K, Peng H, Wen Y and Li N 2010 *Appl. Surf. Sci.* **256** 3093–7

[46] Gong T, Yang D, Hu Y, Yang W, Wang C and Lu J Q 2009 *Colloids Surf.* A **339** 232–9

[47] Cornell R M and Schwertmznn U 1996 *The Iron Oxides: Structure, Properties, Reactions, Occurrence and Uses* (New York: VCH) pp 167–8

[48] Klug H P and Alexander L E 1962 *X-ray Diffraction Procedures for Polycrystalline and Amorphous Materials* (New York: Wiley) pp 491–538